Journal of Alloys and Compounds 739 (2018) 504–509

Contents lists available at ScienceDirect

Journal of Alloys and Compounds

journal homepage: http://www.elsevier.com/locate/jalcom

Sol-gel combustion synthesis of high-quality chromium-doped mixed-metal garnets $Y_3Ga_5O_{12}$ and $Gd_3Sc_2Ga_3O_{12}$

S. Butkute [a, b], E. Gaigalas [c], A. Beganskiene [a], F. Ivanauskas [c], R. Ramanauskas [b], A. Kareiva [a, *]

[a] Institute of Chemistry, Vilnius University, Naugarduko 24, LT-03225, Vilnius, Lithuania
[b] Center for Physical Sciences and Technology, Institute of Chemistry, A. Gostauto 9, LT-01108, Vilnius, Lithuania
[c] Faculty of Mathematics and Informatics, Vilnius University, Naugarduko 24, LT-03225, Vilnius, Lithuania

ARTICLE INFO

Article history:
Received 20 September 2017
Received in revised form
1 November 2017
Accepted 27 December 2017
Available online 29 December 2017

Keywords:
Garnets
GSGG
YGG
Powders
Sol-gel combustion processing
Cr^{3+} doping

ABSTRACT

In this study the chromium-doped (0–20 mol% of Cr^{3+}) garnet structure materials $Y_3Ga_5O_{12}$ (YGG) and $Gd_3Sc_2Ga_3O_{12}$ (GSGG) were synthesized via aqueous sol-gel combustion (SGC) method. The synthesis process was investigated by thermogravimetric (TG) analysis and infrared (IR) spectroscopy. The phase formation at the following synthesis steps was characterized by powder X-ray diffraction (XRD) analysis. Scanning electron microscopy (SEM) was used for the characterization of surface morphology of the end products. Luminescence properties were examined by photoluminescence (PL) spectroscopy and decay time measurements (DT).

1. Introduction

The light emitting diodes (LED's) in now days are the most important light sources, including very specific lightings (healthcare, sensors, data communications, green house farming and etc.) [1]. LED's attract more and more attention because of their sustainability and low energy consumptions [2]. By now not all even visible light region is covered by effective LED lightening. Garnet crystal structure compounds are the most popular host materials for the luminescent centres. A wide range of different elements could be combined in a garnet structure providing a possibility to manipulate with strength of crystal field and resulting to different wavelengths light for the excited element [3–14].

For the preparation of mixed-metal garnets wet chemical synthesis methods, such as sol–gel processing, co-precipitation, glycol-thermal treatment and combustion are very often used [15,16]. Wet chemical synthesis routes provide better control the stoichiometry of the metals and high homogeneity of end products due to the mixing of starting materials at molecular level. Moreover, the decreased synthesis temperatures could be used in comparison with solid-state reaction method. Nevertheless, the sol-gel combustion (SGC) SGC method has advantages among them, such as less time-consuming process, the nano-sized powders with predictable morphology could be obtained, and possibility to obtain high density ceramics with improved luminescence properties [17–19]. Moreover, the mathematical and numerical models of the yttrium aluminium garnet synthesis were presented [20]. The models allowed the effective computer simulation of the YAG synthesis [21,22].

It is well known that luminescent centre of Cr^{3+} emit far-red or near infra-red light, depending on the host lattice. The first solid state laser, in 1960, was made with phosphor Al_2O_3:Cr^{3+} (Ruby). The emission line appeared at around 700 nm caused by $^2E \rightarrow {}^4A_2$ transition [23]. The Cr^{3+} ions ($3\,d^3$) depending on the host crystal field may have different electronic ground states [24]. A relatively large splitting of the ^2E_g state of Cr^{3+} in $Ca_3Al_2(SiO_4)_3$ natural garnet (Grossular) was observed [25]. Recently, the luminescence properties of sol-gel derived GGG:Cr, YGG:Cr, LGG:Cr, and GSGG:Cr doped with different chromium (III) concentrations (3, 5, and 8 mol. %) and annealed at high temperatures (1300 °C, 1400 °C, and 1500 °C) were examined and compared [26]. The optical properties

* Corresponding author.
E-mail address: aivaras.kareiva@chf.vu.lt (A. Kareiva).

https://doi.org/10.1016/j.jallcom.2017.12.332
0925-8388/

of phosphors were found strongly dependent on doping concentration and annealing temperature. The substitution effects of Fe^{3+}, Ce^{3+}, and Ce^{3+}/Cr^{3+} in gallium garnets GGG and GSGG have been also investigated [27]. The highest emission intensity for GGG:Ce^{3+},Cr^{3+} samples containing 3 mol% of dopants (1.5 mol% Ce and 1.5 mol% Cr) was determined. Sol-gel prepared gallium garnets doped with trivalent chromium were characterized by a broad PL band in the far-red region (700–760 nm). This emission meets the needs of photomorphogenesis in plants. Therefore, in this study we continue characterization of sol-gel combustion synthesized $Y_3Ga_5O_{12}$ and $Gd_3Sc_2Ga_3O_{12}$ garnets highly doped with Cr^{3+} (3–20 mol%) investigating the luminescence properties and substitutional limit of chromium doping.

2. Experimental

For the preparation of $Y_3Ga_5O_{12}$ (YGG) and $Gd_3Sc_2Ga_3O_{12}$ (GSGG) doped with Cr^{3+} ions (doping range from 0 to 20 mol%) powder samples the sol-gel combustion method [7] was used. Yttrium oxide (Y_2O_3; 99.99%; Alfa Aesar), gallium oxide (Ga_2O_3; 99.99%; Alfa Aesar), gadolinium oxide (Gd_2O_3; 99.99%; Treibacher Industrie AG), scandium oxide (Sc_2O_3; 99.99%; Treibacher Industrie AG), chromium (III) nitrate nonahydrate ($Cr(NO_3)_3 \cdot 9H_2O$, 99%; Sigma-Aldrich) were used as starting materials. Tris-(hydroxymethyl)-aminomethane (TRIS) ($NH_2C(CH_2OH)_3$; 99.9%; Carl Roth) was used as complexing agents in the sol-gel combustion synthesis. Metal oxides were dissolved in concentrated nitric acid (HNO_3; 65%; Reachem). In the SGC processing, firstly, the stoichiometric amounts of Y_2O_3, Ga_2O_3, Gd_2O_3 and Sc_2O_3 were separately dissolved in boiling concentrated nitric acid. The acidity of these solutions was reduced by evaporating them and diluting with distilled water for 3 times. Then, the obtained metal nitrates solutions were mixed together and with the appropriate volume of $Cr(NO_3)_3 \cdot 9H_2O$ solution in distilled water. Finally, to the above solution the necessary amount of TRIS was added. The TRIS participates in complex formation process and initiates self-burning process as well. After the transparent sol has formed the solvent was slowly evaporated and viscous gel has formed. The formation of gel proceeds during 1 h at 60–75 °C with constant mixing in a partially covered beaker. When the gel was completely dried, the TRIS initiated a spontaneous self-combustion process and either worked as a fuel. After self-initiated combustion crumbly ash-like (Ashen) powders were obtained. Resulting powders were heated at 800 °C (heating rate 1 °C/min) for 5 h. The final annealing was performed for 10 h at 1000 °C (heating rate 3 °C/min.). All synthesized powder samples and their abbreviations, which will be used in this article are summarized in Table 1.

X-ray diffraction (XRD) data were collected in the range of $20 \leq 2\theta \leq 70°$ using Ni-filtered Cu K_α radiation on Rigaku MiniFlex II diffractometer working in Bragg-Brentano ($\theta/2\theta$) geometry. The step width and integration time was 0.02° and 1 s, respectively. The infrared spectra in the range of 4000–400 cm^{-1} were recorded on Perkin-Elmer FT-IR Spectrum BX II FTIR spectrometer equipped with a liquid nitrogen cooled MCT detector. The powder morphology was characterized by scanning electron microscopy (SEM) performed with a Hitachi Tabletop Microscope TM3000. The fluorescence (kinetics, excitation and emission) of synthesized samples was investigated with Fluorescence Spectrometer Edinburgh Instruments FLS980 equipped with double excitation and emission monochromators, 450 W Xe arc lamp, mirror optics for powder samples and liquid nitrogen cooled (−80 °C) NIR detector (Hamamatsu R5509 - 42). Thermogravimetric and differential scanning calorimetry (TG–DSC) analysis was employed to study thermal decomposition process of gels and to determine the phase formation temperature. For thermal experiments the Perkin Elmer STA6000 (Simultaneous Thermal Analyzer) was used (temperature range was from 30 to 1000 °C; the heating rate was 10 °C/min; analysis was performed under flowing (20 ml/min) air atmosphere).

3. Results and discussion

The Y-Ga-O and Gd-Sc-Ga-O precursor gels were characterized by thermogravimetric analysis in the temperature range of 20–1000 °C. Fig. 1 presents TG and DTG curves of YGG Cr15 dried gel. Thermal decomposition of the gel occurs via five main steps of mass loss. The first mass loss is observed between 70 and 150 °C, and corresponds to the dehydration of gel and the beginning of self-combustion reaction. The second three mass loss steps observed in the temperature range of 150–450 °C are associated with main decomposition of organics and metal nitrates [28,29]. With further increasing temperature the mass of the sample is steady till 794 °C. At this temperature, the final decarbonation of metal oxycarbonates takes place among with proceeding of solid state reaction. Interestingly, the thermal decomposition of Y-Ga-O:Cr gels is identical for the samples having different concentrations of chromium. Moreover, thermal behaviour of Gd-Sc-Ga-O precursor gels is also very similar (see Supplement Fig. S1).

The IR spectra of YGG Cr8 samples obtained at different stages of sol-gel combustion processing are presented in Fig. 2. The IR spectrum of dried gel has broad absorption band at 3700-2500 which corresponds O–H vibrations [30]. Absorption bands visible at 2100, 1650 and 1300 cm^{-1} are associated to the stretching in nitrates, carbonates and carboxylates [30,31]. The band located at

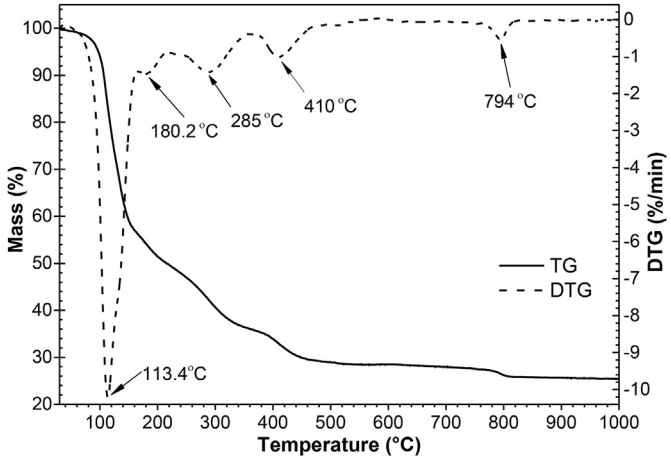

Fig. 1. TG/DTG curves of Y-Ga-O:Cr15% dried precursor gel.

Table 1
The synthesized garnets.

Sample	0 mol %	3 mol %	5 mol %	8 mol %	10 mol %	12 mol %	15 mol %	20 mol %
$Y_3Ga_5O_{12}$ x mol% of Cr^{3+}	YGG	YGG Cr3	YGG Cr 5	YGG Cr8	YGG Cr10	YGG Cr12	YGG Cr15	YGG Cr20
$Gd_3Sc_2Ga_3O_{12}$ x mol% of Cr^{3+}	GSGG	GSGG Cr3	GSGG Cr5	GSGG Cr8	GSGG Cr10	GSGG Cr12	GSGG Cr15	GSGG Cr20

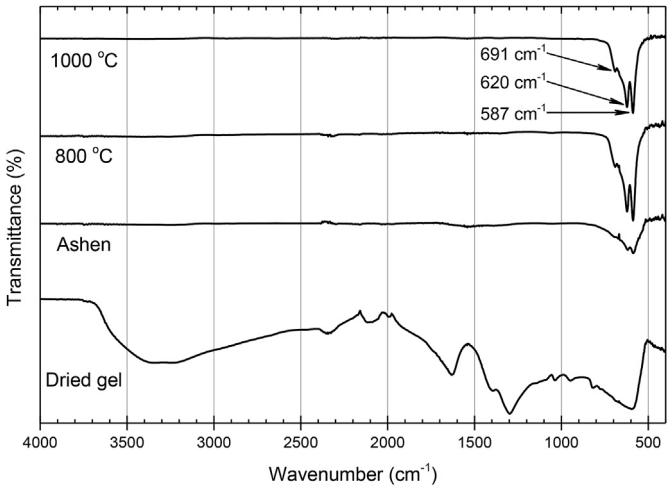

Fig. 2. IR spectra of YGG Cr8 precursor gel and samples annealed at different temperatures.

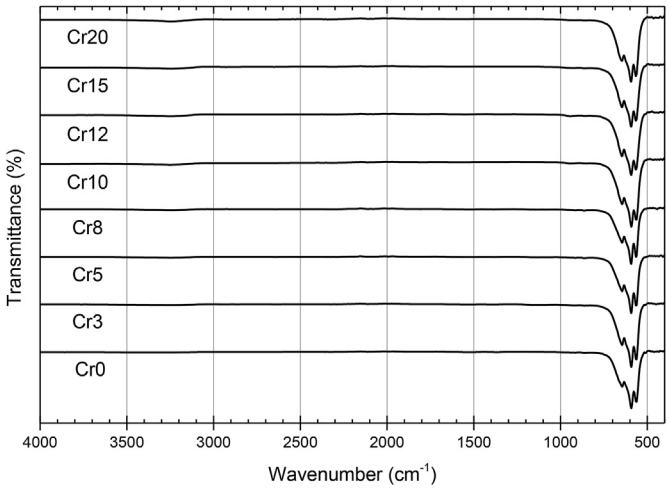

Fig. 4. IR spectra of GSGG:Cr0-20 samples obtained at 1000 °C.

800–500 cm^{-1} can be assigned to the characteristic metal–oxygen vibrations [30–32]. IR spectrum of ashen sample after self-combustion reaction do not have already any absorption bands typical for organic functional groups. The IR spectra of samples annealed at 800 °C and 1000 °C contain only broad absorption band at 800–500 cm^{-1} which is evidently split into the three sharp bands: 691, 620 and 587 cm^{-1}. Such behaviour is typical for the garnet crystal structure materials [16,33,34]. Thus, IR spectroscopy could be used as additional tool for the structural characterization of the garnet materials obtained. The IR spectra of YGG:Cr and GSGG:Cr samples are almost identical between each other and regardless chromium substitutional level (Figs. 3 and 4).

The SEM micrographs of YGG Cr20 and GSGG Cr20 samples are presented in. Fig. 5. The surface morphology of both samples is very similar. The porous solids are composed of plate-like highly agglomerated particles. The level of Cr doping does not influence the morphology of powders as well (see suppl. Figs. S2, S3 and S4).

The XRD patterns of YGG Cr3 samples obtained at different temperatures are shown in Fig. 6. As seen, the crystallization of garnet phase started already after self-combustion reaction. Therefore, this sol-gel combustion synthesis method could be successfully used for the fabrication of doped nanocrystalline ceramics of YAG [35,36]. The broad reflections corresponding to the garnet phase narrowed significantly after additional heating of the sample at 800 °C. Evidently, single-phase garnet phase have formed (PDF2 (ICDD) 00-043-0512), and no any reflections attributable to the impurities could be detected. The diffraction peaks of garnets become much sharper after additional heating of the sample at 1000 °C. The XRD patterns of YGG samples with different substitutional level of chromium and annealed at 1000 °C are presented in Fig. 7. It is clear, that all XRD patterns possess the formation of monophasic samples having garnet crystal structure independently on the amount of substituent element. The same results were obtained in the case of GSGG samples (see Figs. 8 and 9). Again, we can conclude from the XRD results that sol-gel combustion synthesis route gave monophasic GSGG garnets (PDF4 (ICDD) 04-006-8283) in a wide doping concentration range of chromium.

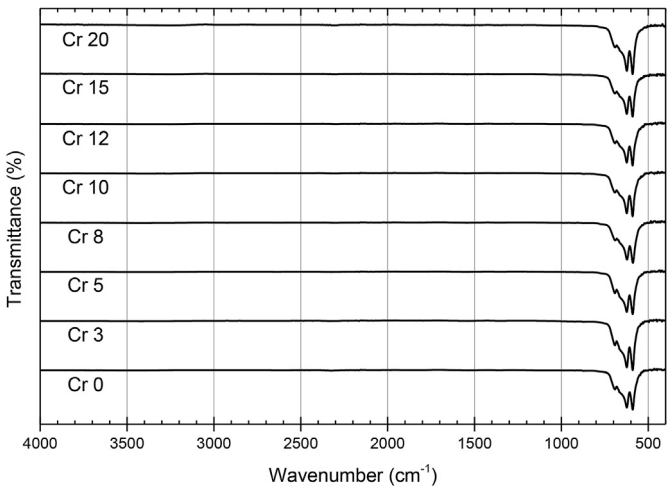

Fig. 3. IR spectra of YGG:Cr0-20 samples obtained at 1000 °C.

The excitation and emission spectra of sol-gel derived YGG and GSGG samples doped with different amount of Cr are given in Figs. 10 and 11, respectively. The excitation spectra of YGG:Cr^{3+} monitored at $\lambda_{em} \approx 710$ nm revealed that the charge transfer (CT) to Cr^{3+} occurs in all samples in the range of 400–700 nm. The excitation in UV and blue spectral regions occurs due to the $^4A_2 \rightarrow {}^4T_1$ transition and that in the red spectral region is due to the $^4A_2 \rightarrow {}^4T_2$ transition [26,37]. It is also evident that the CT energy changes non-monotonically with increasing chromium content in the structure. All YGG:Cr^{3+} powders were excited at 450 nm for taking the emission spectra. The major emission lines are broad and peaked at 715 nm, originating from the $^4T_2 \rightarrow {}^4A_2$ transition. The similar emission at room temperature with the same R-line and two its vibronic side bands was observed by Deren et al. [38]. The highest intensity of emission was observed for YGG:8% Cr^{3+} specimen. The excitation spectra of GSGG:Cr^{3+} samples monitored at $\lambda_{em} \approx 750$ nm is dominated by the same transitions peaked at 450 nm and 620 nm. All powders were excited at 450 nm for taking the emission spectra. The typical Cr^{3+} emission line is observed in the far red spectral region with strong intensity peaked at 750 nm. The highest intensity of $^4T_2 \rightarrow {}^4A_2$ transition was again observed for the GSGG:8% Cr^{3+} specimen. With further increasing chromium content up to 20% the concentration quenching was observed [39,40].

Cr^{3+} concentration dependent decay curves of Cr^{3+}-doped different garnet phosphors are shown in Figs. 12 and 13, respectively. As seen, the decay curves or decay speed of the YGG and GSGG samples are quite similar to each other suggesting similar internal efficiency [41]. It is obvious that decay times for YGG:Cr^{3+}

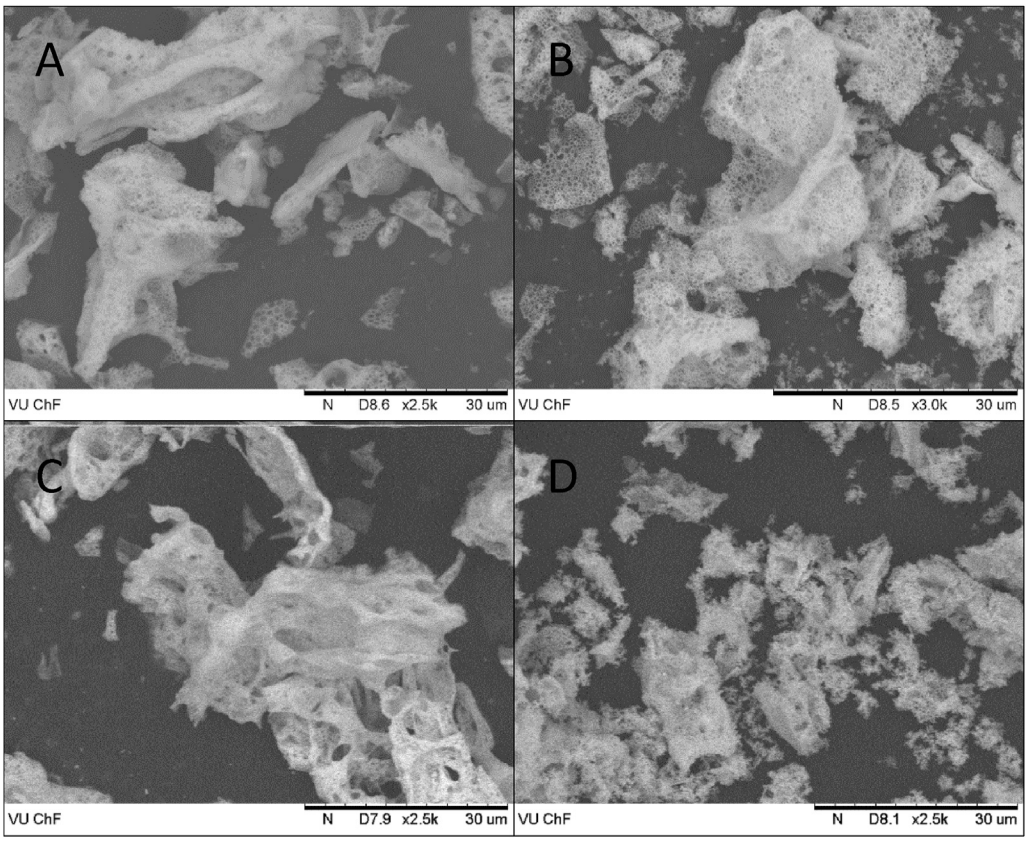

Fig. 5. SEM micrographs of YGG Cr20 and GSGG Cr20 after self-burning (A and C) and after heating at 1000 °C (B and D), respectively.

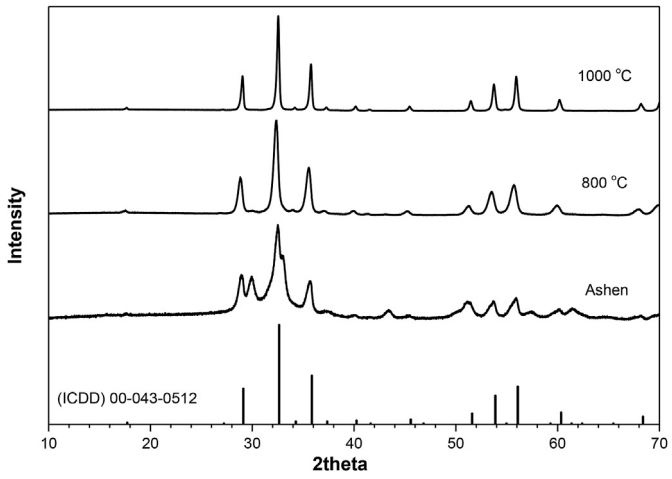

Fig. 6. XRD patterns of YGG Cr3 samples obtained at different temperatures.

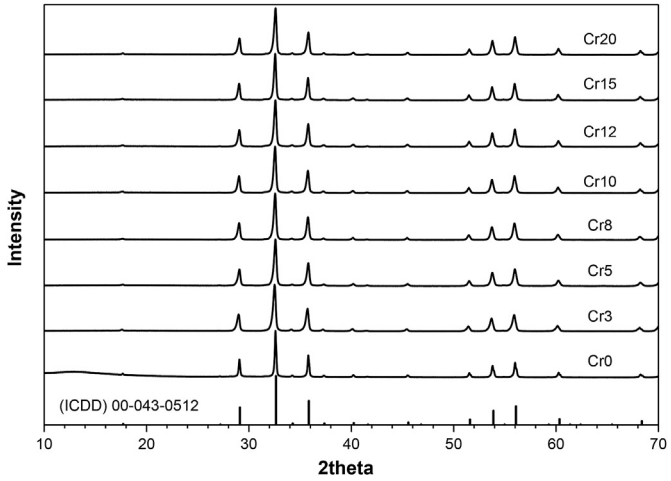

Fig. 7. XRD patterns of YGG samples doped with different amount of Cr and annealed at 1000 °C.

(Fig. 12) and GSGG:Cr^{3+} (Fig. 13) get shorter with higher activator concentration. This can be related with faster energy transfer process between Cr^{3+} ions. However, the decay curves at lower Cr^{3+} concentrations are nearly identical, again suggesting similar internal efficiency of Cr^{3+} ions at low concentrations. Thus, the results reveal the inclusion of trivalent Cr^{3+} ¡n the host lattice. Thus, the doping affects the charge ordering and hence on the material's optical behaviour [42,43]. The advantages of Cr:YGG and Cr:GSGG luminescent powders compared with others that emit far-red or near infra-red light are chemically inert and very stable at high temperatures host matrix, lower chromium quenching effect on the emission in the garnet matrixes and higher emission intensity with higher activator concentration. Therefore, these phosphors could be successfully used for the plant development controlled by light.

4. Conclusions

In this study the chromium-doped garnet structure materials $Y_3Ga_5O_{12}$ (YGG) and $Gd_3Sc_2Ga_3O_{12}$ (GSGG) were synthesized using aqueous sol-gel combustion method. It was determined, that thermal decomposition of Y-Ga-O:Cr gels was identical for the

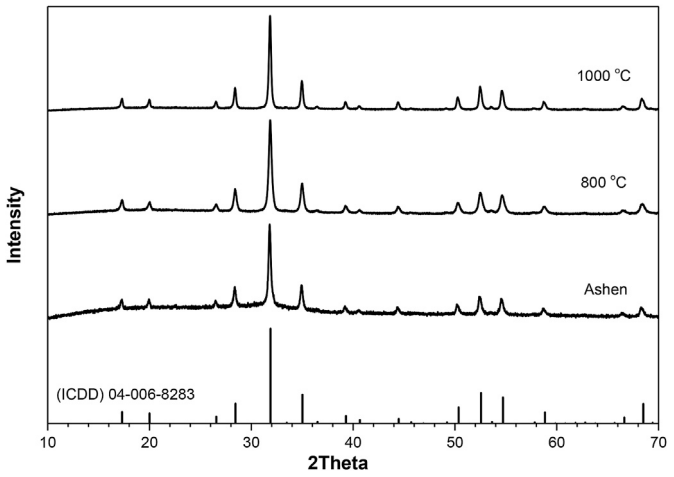

Fig. 8. XRD patterns of GSGG Cr10 samples obtained at different temperatures.

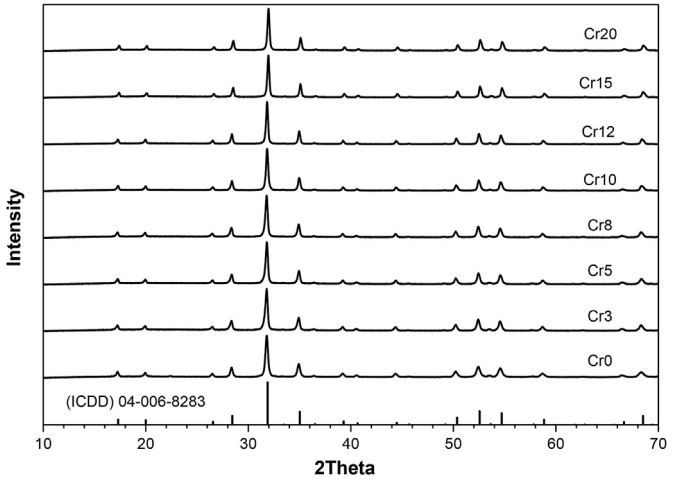

Fig. 9. XRD patterns of GSGG samples doped with different amount of Cr and annealed at 1000 °C.

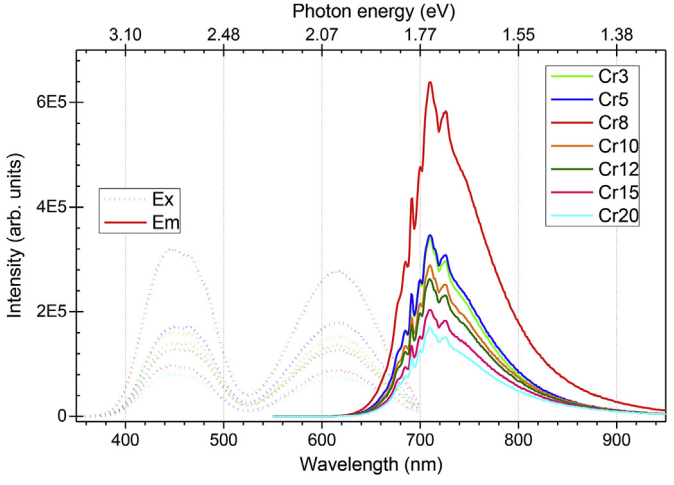

Fig. 10. Excitation (Em = 710 nm) and emission (Ex = 450 nm) spectra of YGG:Cr^{3+} samples.

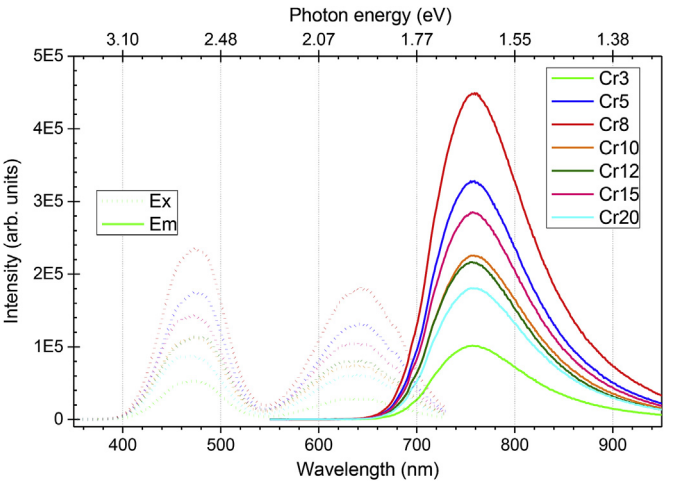

Fig. 11. Excitation (Em = 750 nm) and emission (Ex = 450 nm) spectra of GSGG:Cr^{3+} samples.

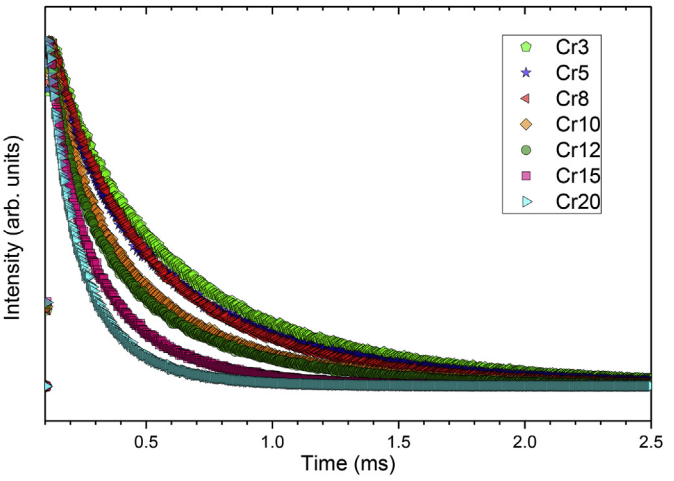

Fig. 12. Decay curves of YGG:Cr^{3+} samples as a function of Cr^{3+} concentration.

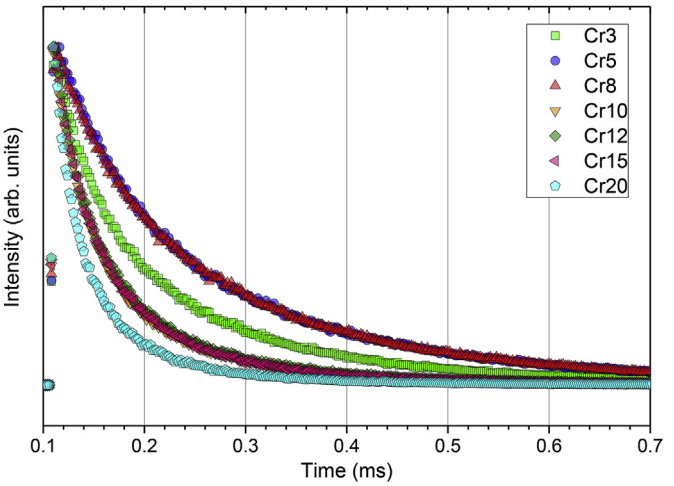

Fig. 13. Decay curves of GSGG:Cr^{3+} samples as a function of Cr^{3+} concentration.

samples having different concentrations of chromium and similar to the thermal behaviour of Gd-Sc-Ga-O precursor gels. The IR spectra of samples annealed at 1000 °C contained only broad absorption bands at 800–500 cm^{-1} which was split in to the three

sharp bands 691, 620 and 587 cm^{-1} typically assigned for the garnet crystal structure materials. From these and the XRD results was concluded that sol-gel combustion synthesis route gave monophasic YGG and GSGG garnets in a wide doping concentration range of chromium. The surface morphology of both YGG:Cr^{3+} and GSGG:Cr^{3+} samples was found to be very similar. The porous solids were composed of plate-like highly agglomerated particles. The major emission lines of YGG:Cr^{3+} samples were peaked at 715 nm, originating from the $^4T_2 \rightarrow {}^4A_2$ transition. For the GSGG:Cr^{3+} samples the typical Cr^{3+} emission line was observed in the far red spectral region with strong intensity peaked at 750 nm. In both garnets, the highest intensity of $^4T_2 \rightarrow {}^4A_2$ transition was observed for YGG:8% Cr^{3+} and GSGG:8% Cr^{3+} specimens. With further increasing chromium content up to 20% the concentration quenching was observed. The decay curves of the YGG and GSGG samples were quite similar to each other. The decay times for YGG:Cr^{3+} and GSGG:Cr^{3+} were shorter with higher activator concentration. However, the decay curves at lower Cr^{3+} concentrations were nearly identical, suggesting similar internal efficiency of Cr^{3+} ions.

Acknowledgements

This work was supported by Lithuanian-French grant (Registration No. TAP LZ-17-009) from the Research Council of Lithuania.

Appendix A. Supplementary data

Supplementary data related to this article can be found at https://doi.org/10.1016/j.jallcom.2017.12.332.

References

[1] T. Dierkes, J. Plewa, T. Juestel, J. Alloy. Comp. 693 (2017) 291–302.
[2] S. Moeller, A. Katelnikovas, M. Haase, T. Juestel, J. Lumin. 172 (2016) 185–190.
[3] G. Blasse, J. Deblank, D.J.W. Ijdo, Mater. Res. Bull. 30 (1995) 845–850.
[4] V.J. Pugh, F.S. Richardson, J.B. Gruber, M.D. Seltzer, J. Phys. Chem. Solid. 58 (1997) 85–101.
[5] A. Leleckaite, A. Kareiva, Opt. Mater. 26 (2004) 123–128.
[6] F. Piccinelli, A. Speghini, G. Mariotto, L. Bovo, M. Bettinelli, J. Rare Earths 27 (2009) 555–559.
[7] A. Kaminska, A. Duzynska, M. Berkowski, S. Trushkin, A. Suchocki, Phys. Rev. B 85 (2012), 155111.
[8] R. Skaudzius, J. Pinkas, R. Raudonis, A. Selskis, R. Juskenas, A. Kareiva, Mater. Chem. Phys. 135 (2012) 479–485.
[9] A. Katelnikovas, S. Sakirzanovas, D. Dutczak, J. Plewa, D. Enseling, H. Winkler, A. Kareiva, T. Juestel, J. Lumin. 136 (2013) 17–25.
[10] X. Ding, G. Zhu, W.Y. Geng, Q. Wang, Y.H. Wang, CrystEngComm 17 (2015) 3235–3242.
[11] J.Y. Zhong, W.D. Zhuang, X.R. Xing, R.H. Liu, Y.F. Li, Y.H. Liu, Y.S. Hu, J. Phys. Chem. C 119 (2015) 5562–5569.
[12] X. Teng, J.K. Li, G.B. Duan, Z.M. Liu, J. Lumin. 179 (2016) 165–170.
[13] M. Colmont, S. Saitzek, A. Katelnikovas, H. Kabbour, J. Olchowka, P. Roussel, J. Mater. Chem. C 4 (2016) 7277–7285.
[14] A.G. Petrosyan, H.R. Asatryan, K.L. Hovhannesyan, M.V. Derdzyan, S.P. Feofilov, A.V. Eganyan, R.S. Sargsyan, Mater. Chem. Phys. 185 (2017) 39–43.
[15] Y.B. Chen, J. Wang, M.L. Gong, Q. Su, J.X. Shi, Chem. Lett. 36 (2007) 760–761.
[16] A. Kareiva, Mater. Sci.(Medžiagotyra) 17 (2011) 428–437.
[17] H.L. Li, X.J. Liu, L.P. Huang, Opt. Mater. 29 (2007) 1138–1142.
[18] A. Katelnikovas, H. Bettentrup, D. Uhlich, S. Sakirzanovas, T. Justel, A. Kareiva, J. Lumin. 129 (2009) 1356–1361.
[19] A. Zarkov, A. Stanulis, T. Salkus, A. Kezionis, V. Jasulaitiene, R. Ramanauskas, S. Tautkus, A. Kareiva, Ceram. Int. 42 (2016) 3972–3988.
[20] F. Ivanauskas, A. Kareiva, B. Lapcun, J. Math. Chem. 46 (2009) 427–442.
[21] M. Mackevicius, F. Ivanauskas, A. Kareiva, I. Bogdanoviciene, J. Math. Chem. 51 (2013) 1249–1257.
[22] J.A. Caballero, M.A. Navarro, R. Ruiz-Femenia, I.E. Grossmann, Appl. Energy 124 (2014) 256–273.
[23] G. Blasse, B.C. Grabmaier, Luminescent Materials, Springer-Verlag, Berlin ; New York, 1994.
[24] M. Yamaga, A. Marshall, K.P. O'Donnell, B. Henderson, Y. Miyazaki, J. Lumin. 39 (1988) 335–341.
[25] Z. Mazurak, Opt. Mater. 3 (1994) 89–93.
[26] A. Zabiliute, S. Butkute, A. Zukauskas, P. Vitta, A. Kareiva, Appl. Optic. 53 (2014) 907–914.
[27] S. Butkute, A. Zabiliute, R. Skaudzius, P. Vitta, A. Beganskiene, A. Zukauskas, A. Kareiva, J. Sol. Gel Sci. Technol. 76 (2015) 210–219.
[28] P. Melnikov, V.A. Nascimento, L.Z.Z. Consolo, A.F. Silva, J. Therm. Anal. Calorim. 111 (2013) 115–119.
[29] P. Melnikov, V.A. Nascimento, I.V. Arkhangelsky, L.Z.Z. Consolo, L.C.S. de Oliveira, J. Therm. Anal. Calorim. 114 (2013) 1021–1027.
[30] X.X. Li, T. Odoom-Wubah, Z.X. Chen, B.Y. Zheng, H.L. Huang, Ceram. Int. 40 (2014) 16317–16321.
[31] S. Saxena, K.A. Asokkumar, B. Lal, J. Sol. Gel Sci. Technol. 41 (2007) 245–248.
[32] X.X. Li, W.J. Wang, Powder Technol. 196 (2009) 26–29.
[33] P. Vaqueiro, M.A. Lopez-Quintela, Chem. Mater. 9 (1997) 2836–2841.
[34] N. Dubnikova, E. Garskaite, A. Beganskiene, A. Kareiva, Opt. Mater. 33 (2011) 1179–1184.
[35] A. Speghini, F. Piccinelli, M. Bettinelli, Opt. Mater. 33 (2011) 247–257.
[36] R. Tomala, L. Marciniak, J. Li, Y.B. Pan, K. Lenczewska, W. Strek, D. Hreniak, Opt. Mater. 50 (2015) 59–64.
[37] S. Kurosawa, A. Suzuki, A. Yamaji, K. Kamada, J. Pejchal, Y. Ohashi, Y. Yokota, V.I. Chani, A. Yoshikawa, J. Cryst. Growth 452 (2016) 95–100.
[38] P.J. Deren, A. Watras, A. Gagor, R. Pazik, Cryst. Growth Des. 12 (2012) 4752–4757.
[39] J. Pareja, C. Litterscheid, A. Molina, B. Albert, B. Kaiser, A. Dreizler, Opt. Mater. 47 (2015) 338–344.
[40] X.M. Zhu, Y.L. Yao, Z.F. Zhou, Opt. Mater. 62 (2016) 104–109.
[41] A. Stanulis, A. Katelnikovas, M. Van Bael, A. Hardy, A. Kareiva, T. Justel, J. Lumin. 172 (2016) 323–330.
[42] D. Yan, B. Lei, B. Chen, X.-J. Wu, Z. Liu, N. Li, J. Ge, Y. Xue, Y. Du, Z. Zheng, H. Zhang, Appl. Mater. Today 1 (2015) 20–26.
[43] T.K. Thirumalaisamy, S. Saravanakumar, S. Butkute, A. Kareiva, R. Saravanan, J. Mater. Sci. Mater. Electron. 27 (2016) 1920–1928.